2026 Collegiate Wind Competition
Turbine Design and Testing Report
April 23, 2026

Massachusetts Institute of Technology (MIT)
Cambridge, Massachusetts

Faculty Advisor: Michael Howland (mhowland@mit.edu)
Team Mentor: Kirby Heck (kheck@mit.edu)
Social Media: https://www.instagram.com/mitwindclub/

Team Members

Build Team Lead: Angelica Knudsen (aknudsen@mit.edu)
Build Members: Logan Reich (lreich@mit.edu), Lila Shelton (lshelton@mit.edu), Matthew Nuñez (nunez634@mit.edu)

Acknowledgments

Mentor: Kirby Heck (kheck@mit.edu)

Table of Contents

1: Executive Summary

The MIT Wind Team designed a small-scale, three-bladed, horizontal-axis, onshore wind turbine for the 2026 Collegiate Wind Competition.

The blade mechanical system consists of turbine blades on a fixed pitch mount, attached to a metal axle via a support mounting, which is attached to a generator. We selected the NACA 4412 airfoil for our turbine blades due to its superior lift at lower speeds, and manufactured it via 3D printing of polylactic acid (PLA). PLA was chosen as the blade material because it is readily available, lightweight, and easily reprinted for iterative design. Set screws are used to hold the blades at a fixed pitch on the rotor hub, which is attached via a shaft coupler to the generator shaft. The tower consists of a steel flange welded to a steel tube, which is connected to the turbine tower. The nacelle, which is laser cut from acrylic, is mounted to the top of the turbine tower with a PLA flange.

The electrical system consists of a power flow circuit and a data flow circuit. The power flow is from a generator to a 3-phase rectifier and then through a point of common coupling (PCC) to a parallel variable resistor array. The data flow is from the optical encoder and emergency stop (E-stop) brake signal to an Arduino Uno serving as a microcontroller, which in turn controls the braking circuit and the parallel variable resistor array. We chose to use a BL23E22-02 standard Brushless Direct Current (BLDC) motor as our generator due to its high efficiency and ease of integration. For our rectifier, we used a full bridge rectifier made of six diodes to rectify the power and reduce variability, followed by an array of parallel MOSFET-controlled resistors to vary the resistance and reach a power-maximizing point. These were both chosen due to their simple and resilient structure and high efficiency. An open-loop control algorithm is run by an Arduino Uno microcontroller to control both the resistance and activate the brake system. In turn, the brake system short-circuits the load and thus increases the self-induced torque in the generator, and activates a manual brake pad on a motor to slow the rotation.

These design choices are a modification of the MIT Wind design from last year, focusing on streamlining operations to reduce points of failure and ensuring a resilient system. In addition, the tower, foundation, and nacelle mounting were redesigned to account for this year's focus on onshore turbines.

1.1: Design Objectives

The design objectives this year were threefold: effective power production, safety, and minimal points of failure. These objectives were chosen to reflect the competition objectives related to power maximization and safety, as well as accounting for MIT Wind's specific challenges in design failures last year. Our success in these goals can be measured by whether we generate measurable power, implement a multimodal braking system and meet safety requirements, and are able to successfully replicate tests using the full turbine setup without failure.

As part of the first goal of maximum power production, we chose an effective blade design, a high-efficiency generator, and power electronics focused on minimizing losses. Specifically, the blade objective was to choose the most efficient blade design that could handle the mechanical stresses from thrust and centrifugal forces while being manufacturable using lightweight material. The axle mounting system was chosen to reduce mechanical loss points. Likewise, multiple potential generator designs were profiled using a dynamometer to choose the most efficient one. For the power electronics system comprising the rectifier and variable parallel resistance array, the goal was power maximization, voltage control, rectification, and signal smoothing while reducing losses for a low-voltage application. Similarly, the corresponding controller objective was to minimize power draw while maximizing net power production.

The safety objective includes three components: mechanical safety, electrical safety, and the braking system.

Mechanical safety involves avoiding excess stress that would cause plastic deformation of mechanical components. Each mechanical component is subjected to different loading and possible failure modes. The rotor blades and hub are designed to avoid yielding at high rotation rates due to centripetal acceleration. With the nacelle, a stiff base plate is used to keep the generator shaft aligned with the rotor and to limit low-frequency vibrational modes. Lastly, for the tower and foundation, this involves not bending due to the asymmetric forces on the turbine.

Electrical safety involves using organized power and data cables with quick connectors, separate and optically isolated NEMA-compliant turbine and load boxes, ensuring thorough grounding, and appropriately power rated wires and resistors. To avoid excess stress on wires, a design goal was set to ensure safe minimal wire turn radio, and firm wire securing on the turbine itself. Box objectives were set to meet those requirements, as well as for grounding and sufficiently sized power electronics equipment.

The braking system's objective was rapid braking without interfering with normal turbine operation, and a repeatable braking system. This included both mechanical and electrical braking components that work in tandem to improve performance and robustness.

Our final goal was associated with reducing points of failure, associated with specific concerns about the design from last year. Practically, this led to a design objective for the simplest solution meeting the performance objectives while minimizing the number of components. A specific focus was placed on reducing the number and complexity of actively controlled and/or moving components, which were a source of failure in last year's design.

1.2: Comparison to Prior Years' Designs

Our priority this year was increasing the robustness and simplicity of the wind turbine. For robustness, we drastically reduced the cantilevering of both the base and shaft of the rotor. This was done by placing the top flange of the tower closer to the center of mass of the nacelle. The fixed pitch shortens the shaft length, reduces points of failure in the system, and simplifies the electrical controls. For ease of building, we used M4 screws wherever possible.

On the electrical side, we sought to simplify the variable load control. To do so, we created a simple mapping function that relates measured RPM to ideal resistance for maximum power output. The Power-RPM-Resistance curve was obtained to find the optimal resistance at a given RPM. Last year, we attempted using a MOSFET as a variable resistor, which proved unstable across the full range of voltages output by the turbine. For increased reliability, we now have a parallel resistor array with MOSFETs, where discrete resistance values can be achieved depending on which MOSFETS are turned on.

2: Mechanical

The mechanical system consists of primary sections: the nacelle and the tower. On the nacelle, a 3D printed rotor held in place with a 3D printed and acrylic hub is attached on a metal axle to a support mounting, and is then attached to the generator via a shaft coupler. This equipment rests on stacked acrylic plates. The tower consists of a steel tube with a 3D printed flange on the top, and is welded to a metal flange on the bottom. All computer-aided design (CAD) was done in Solidworks [1].

Figure 1: CAD of full turbine assembly. The main components are the rotor, nacelle, foundation, and braking system.

2.1: Rotor

The components of the rotor are the hub, 6 mm steel drive shaft, 6 mm x 8 mm shaft coupler, and generator, shown in figure 2a. The subcomponents of the hub are the hub coupler, blade holders, acrylic plates, and the blades, pictured in figure 2b. The hub coupler secures the hub to the shaft with an M4 set screw. The blade holders each have an M4 screw that screws into the cylindrical blade base.

For blade design, we used QBlade. The NACA 4412 airfoil for the blade cross-section was chosen due to its superior lift at lower speeds [2]. The team implemented a swept area diameter of 0.45 m, the max possible diameter, to maximize power output. The specific parameters input into QBlade are: blade length of 0.21 m, hub radius of 0.01 m, and tip-speed ratio of 3.5. We also widened the default chord length of QBlade's blade design to increase blade strength.

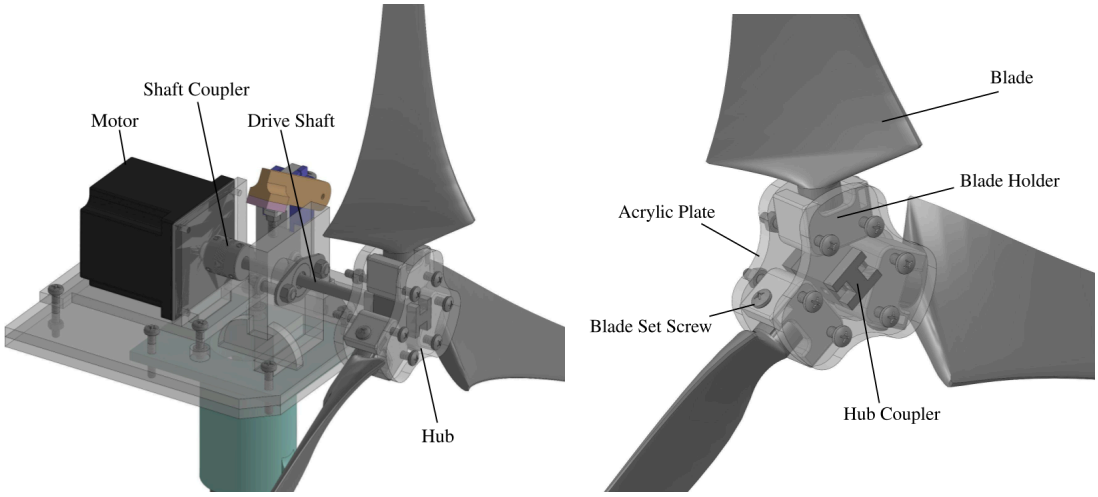

(a) (b)

Figure 2: (a) Components of the rotor and (b) subcomponents of the hub.

2.1.1: Performance

Using QBlade, we simulated the performance of the blades with a variety of possible pitch angles. Specifically, we were interested in comparing the coefficient of performance (C_p) to the tip-speed ratio (TSR). From figure 3, a pitch of 4° appears to be optimal, which we select as the fixed blade pitch in the rotor assembly.

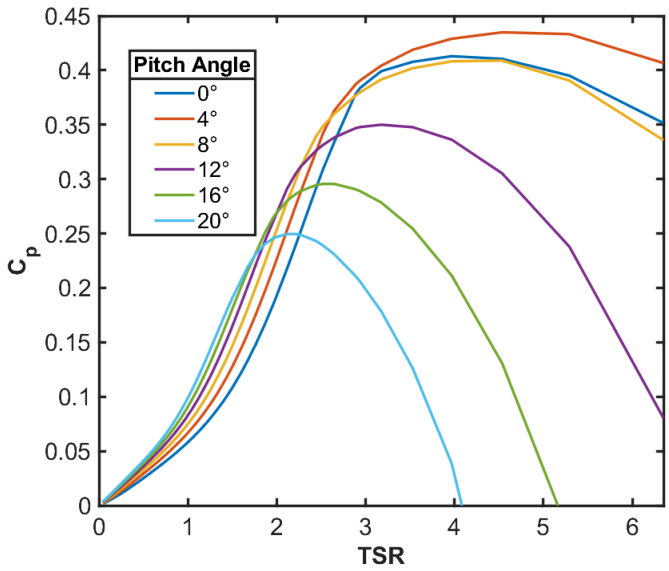

Figure 3: Plot of C_p versus TSR for a variety of pitch angles ranging from 0° to 20°.

2.1.2: Loads and Safety Factors

The main loads to consider are centrifugal forces on the blades. The filament we use is PLA, which has a tensile strength of 50 MPa [3]. When 3D-printed, a PLA part will likely have a tensile strength closer to 5 MPa due to the infill percentage. With our safety factor of 1.5, we should not exceed 3.3 MPa. From testing in the wind tunnel, the maximum RPM is roughly 2800 RPM, where the angular velocity ω = 293 rad/s, leading to a theoretical maximum centrifugal

force on the blades to be 300 N. This is quite significant, so we opted to 3D-print the blades with the filament layer lines oriented along the blade in the $\hat{\jmath}$ direction, indicated in figure 4, to increase blade strength. This is because 3D-printed materials are anisotropic and strongest along the length of the extruded filament [4]. From the free-body diagram analysis in figure 3, we find that the cross-section of the weakest point will experience a theoretical maximum stress of 1.6 MPa, giving a factor of safety of 3.1.

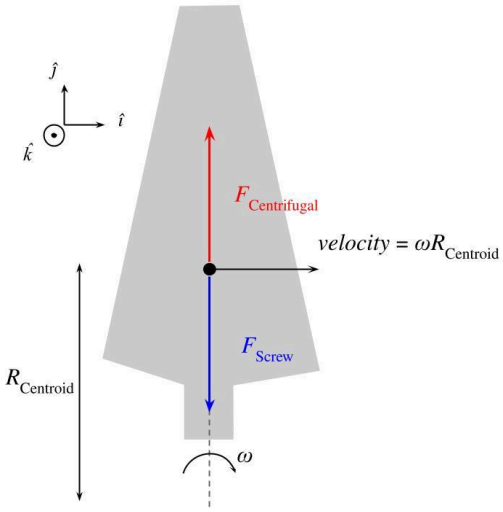

Figure 4: Free body diagram of forces on the blade. The max force the screw must hold is the centripetal force $F_{Screw} = m_{blade}\omega_{max}^2 R_{Centroid}$, with ω_{max} = 293 rad/s, m_{blade} = 42 grams, and $R_{Centroid}$ = 8.32 cm. This results in F_{Screw} = 300 N.

2.2: Nacelle and Foundation

The nacelle is made out of laser cut 6 mm thick acrylic pieces that are epoxied together. For added robustness, the base and flange bearing holder were made of two stacked acrylic pieces. The generator mount was made detachable with vertical screws to streamline the assembly process.

For the foundation, we used a 1.5" diameter steel tube, per competition regulations. It is sufficiently wide to run the electrical wiring through the center and out through the bottom of the base flange. The base flange is composed of another steel tube that surrounds the tower tube, which is then welded to a ¼" thick, 6" diameter steel disc. The disc has three drilled holes to accommodate the three M10 mounting studs for the tunnel testing at the competition.

2.2.1: Loads

The main load on the nacelle will be due to axial thrust from the wind [5]. The formula for the axial thrust F_{Thrust} is

$$F_{Thrust} = \frac{1}{2} C_T \rho U^2 A,$$

where C_T is the coefficient of thrust, ρ is the density of air, U is the freestream wind speed, and A is the rotor swept area [6]. We estimate axial loads using the Betz-optimal thrust coefficient C_T is 8/9 and a wind speed U = 13 m/s, which is the maximum power-generating wind speed for the competition. Using ρ = 1.225 kg/m^3 and A = 0.159 m^2 results in a theoretical maximum F_{Thrust} of 14.6 N. As the axial thrust force is an order of magnitude less than the centrifugal force on the blades, we do not include the axial force in the blade design. The axial thrust force also exerts a

moment on the base flange of 8.8 N-m, which induces stresses well below the yield stresses in the welded steel base.

2.3: Braking System

For braking, we use a ROB-09065 SparkFun servo that actuates an arm to press a brake pad against the shaft to increase rotational friction and slow the rotor. It is activated when the optical encoder in the generator detects an RPM above the 2800 RPM threshold or when the emergency stop button is pressed. The servo is held in place with the clamp and two M4 screws. The brake base is then screwed into the acrylic base plate with two additional M4 screws. The arm is a 3D-printed attachment with a piece of rubber for increased friction.

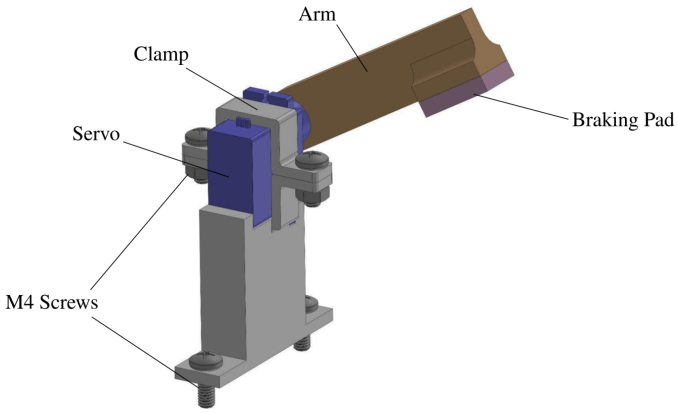

Figure 5: Diagram of braking mechanism.

2.3.1: Performance

The servo supplies a torque of 0.12 N-m [7]. The distance between the servo and the shaft is 5 cm, leading to a force of 2.4 N exerted on the shaft. The braking pad consists of rubber glued to the servo arm. From testing in the wind tunnel, the introduced friction has been proven to sufficiently slow the rotor to a safe limit.

3: Electrical and Controls

The electrical system includes the turbine electronics, the turbine box, and the load box. The power flow begins in the turbine nacelle, where three-phase AC power is generated. This AC signal is then rectified into DC power via a 3-phase full bridge rectifier within the turbine box, and then flows through the Point of Common Coupling (PCC). A parallel variable resistor array is used as a load to dissipate the power. This array is controlled via an Arduino Uno microcontroller, which receives data from the optical encoder and the external E-stop signal. The Arduino Uno also controls the braking circuit servo. Further, an optocoupler is used to optically isolate the data in the two boxes from each other.

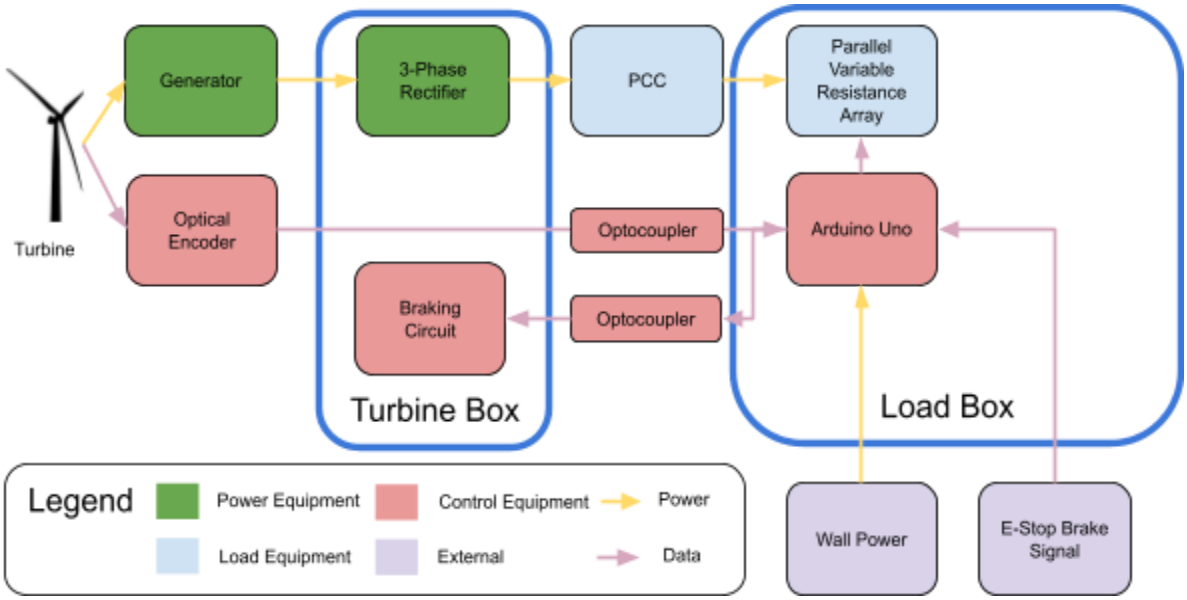

Figure 6: High-level schematic of the electronic system.

3.1: Power Flow Electronics

The overall power flow path is from the generator, then exported along a grounded cable bundle within the turbine shaft, to a fast-charging Universal Service Bus (USB) power adapter cable, which connects to the turbine box. Within the turbine box, a 3-phase bridge rectifier is used to convert the AC power into DC power, which is then transmitted along another USB cable to the load box, where it is passed through a parallel variable resistance array that dissipates power. We implemented a buck-boost converter to limit the voltage and current to be 48V DC and 2A DC to stay within the competition limits.

3.1.1: Generator

We used a D6374 150 kV dual-shaft ODrive motor to drive two different candidate motors and evaluate their performance as generators, and then selected one. Based on the results of a Python script used to calculate efficiency, the BL23E22-02 standard BLDC motor exhibited the highest average efficiency over time and was thus chosen. Efficiency was calculated as:

$$Eff(\%) = \frac{P(generator)}{P(odrive)} \cdot 100$$

In addition, the generator was profiled using a dynamometer to map the power surface over RPM and resistance, which was used in the open control loop described in 3.3.1.

3.1.2: 3-Phase AC Bridge Rectifier

The 3-phase rectifier utilizes six diodes, arranged in two sets of three. These diodes solely allow current to pass during the peak phase, which changes every 60 degrees, reducing the variability by increasing the frequency of circuit harmonics by 6. The switch between the set of three diodes corresponding to the positive phase and three corresponding to the negative phase also leads to rectification and an overall smooth DC output. This system is highly efficient, commonly used in power electronics, and avoids the need for a neutral wire [8].

3.1.3: Parallel Variable Resistor Array

The parallel variable resistor array allows for controlling the resistance to lead to the power-maximizing point. We took inspiration from Cal Maritime's 2024 report when designing this system [9]. Compared to a buck-boost converter system to control the voltage or a singular variable resistor, such an array reduces the switching noise, improves precision, and reduces points of failure (as each resistor is a static fixed resistance). The effectiveness is also comparable for low-power applications such as this one. Specifically, this array includes high-power rated resistors placed in parallel and controlled via Metal Oxide Semiconductor Field Effect Transistors (MOSFETs), which in turn are controlled via digital signals from an Arduino Uno microcontroller and protected via a fixed resistance. These are then attached to a fixed load, serving as the power output.

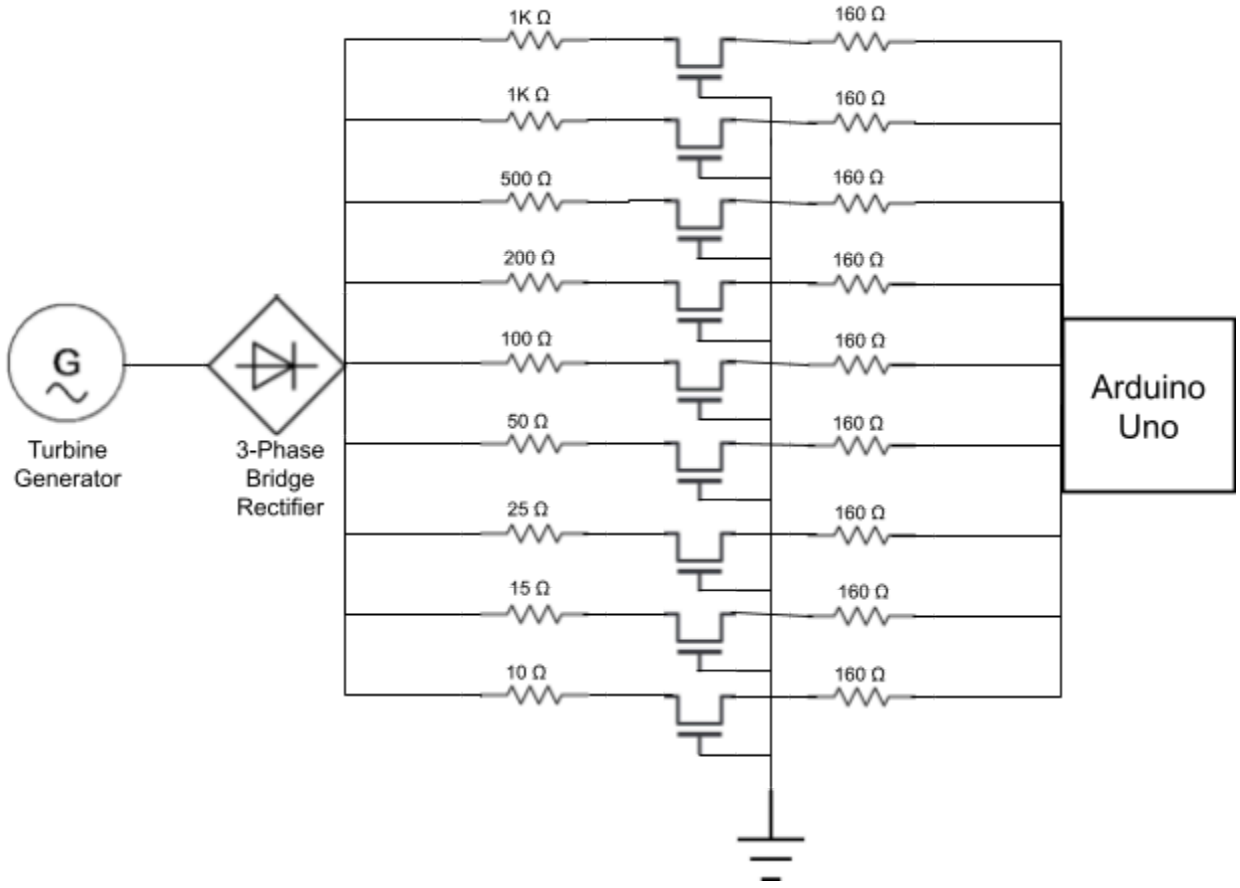

Figure 7: Circuit diagram for power system, including the parallel variable resistor array.

The nine resistor values in parallel were determined through trial and error. They are roughly factors of two from one another, which produces a nice spread of possible resistance values, as pictured in figure 8.

Figure 8: Resistance spread showing the discrete resistances achievable in the variable resistance array.

3.2: Data Flow Electronics

All data flows, namely the power reading, optical encoder reading, and e-stop signals, pass into the Arduino Uno microcontroller, which outputs control signals into the parallel variable resistance array and through the optocoupler to the braking circuit [10]. The optical encoder attached to the generator uses a light source and a rotating disk with slits to count the rotations per minute (RPM) of the generator, and sends this information to the Arduino Uno. The braking circuit contains a simple servo motor attached to a brake pad, which is triggered by activation of the power signal from the Arduino Uno itself. A generic optocoupler is used to optically isolate the braking circuit from the Arduino, preventing electrical noise in the power flow from triggering the brake or contaminating the data flow.

3.3: Controls

The control system includes two feedback processes: a variable resistance controller and a safety activation controller, as shown in figure 9. The variable resistance controller is dependent on an RPM signal from the optical encoder. Similarly, the safety controller is dependent on either the external E-stop signal or dangerous RPM input signals level. This produces a simple on/off state where either the full safety system is activated, or none is. All software is tested on the full range of potential signals, via induced external forcings programmed into a test software to simulate external conditions, as well as full-system testing using the external sensors. Error handling states, where nothing is changed, were also included to prevent erroneous signals or other unexpected issues.

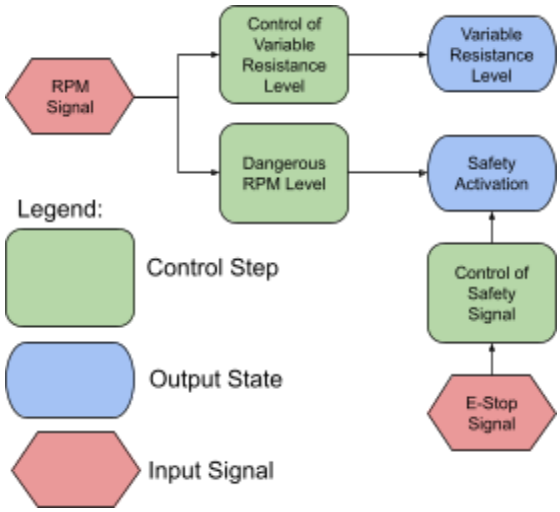

Figure 9: State machine control diagram, demonstrating control flows and activations.

3.3.1: Power Electronics Controls

RPM and power level readings are evaluated based on the following optimization surface in Figure 8. This plot was interpolated from empirical tests of power readings at five different resistance levels and five different RPM using makima interpolation, as gathered by manual readings using the custom-built dynamometer. At each RPM level, a precomputed lookup table is used to determine the optimal combination of MOSFETs to activate to reach the maximal power output. Based on the inferred power and controlled resistance values, the voltage can also be evaluated. The voltage is being evaluated from inferred power rather than direct measurement to reduce complexity and prevent extra inputs to the microcontroller. This system also allows us to vary the resistance to control the voltage in the circuit, and ensure it remains within a safe range, namely below 48V.

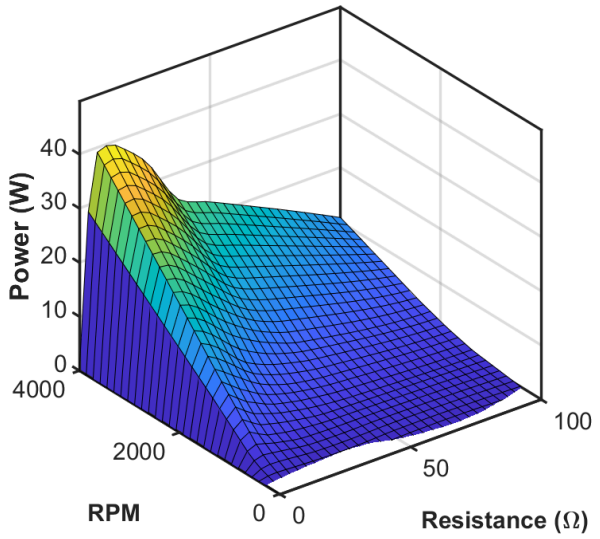

Figure 9: RPM-Power-Resistance curve for power electronics control and voltage regulation. The data past 2800 RPM is extrapolated.

3.3.2: Braking System Controls

E-stop signals or RPM levels rising beyond 2800 trigger the safety braking procedure, which consists of activating the braking circuit, and sending the braking signal to the parallel variable resistor array. The braking circuit activation triggers moving the brake pad onto the axle, slowing down the rotation. In addition, the brake signal triggers shutting off all resistors and short-circuiting the generator, leading to inductive resistance which further slows down the rotation. Combined, these two factors lead to an effective braking system and prevent reliance on a single point of failure.

4: Assembly, Operation, and Testing

4.1: Assembly

The main mechanical assembly in the wind tunnel will be securing the base flange to the M10 mounting studs. The nacelle and tower will be rotated such that the turbine faces normal to the incoming wind direction. The electrical wiring will be fed through the bottom hole, where the power and data cables will be fed through the tunnel door and connected to the turbine-side electronics.

4.2: Commissioning Checklist

The commissioning checklist includes four primary check areas: mechanical, electrical, software, and integration.

First comes the mechanical checks:

1. Checking screws and nuts to prevent parts from coming off, particularly the set screws
2. Checking all materials for signs of deformation or degradation, particularly the blades
3. Check for signs of warping in the axle, blades, or nacelle mount
4. Check for any brakes in the wire coatings, excess stress, or gaps in the electrical boxes
5. Perform a manual spin test of the blades to test rotation and alignment
6. Check blade pitch levels

Then, comes the electrical checks, as some of these rely on mechanical systems:

1. Check flow of power through all resistor options in the resistor array
2. Check successful rectification of power in the rectifier
3. Check successful activation of the braking circuit
4. Check successful powering of the Arduino Uno
5. Check ability of the Arduino to control the MOSFETs

Next, comes the software or control system checks, which rely on the electrical and mechanical systems:

1. Within software sandbox, check at five points (including endpoints) the power resistor activation signals
2. Within software sandbox, check E-stop activation of braking signals
3. Within software sandbox, check excess RPM activation of braking signals
4. Outside of software sandbox, check at five points (including endpoints) the power resistor activation signals
5. Outside of software sandbox, check E-stop activation of braking signals
6. Outside of software sandbox, check excess RPM activation of braking signals

Lastly, the integration checks, where an end-to-end system check is run involving full testing of the mechanical system in the turbine, the electrical system, the resistance control system, and the E-stop braking system.

4.3: Testing

We tested the turbine using the MIT AeroAstro Department's open flow wind tunnel and recorded the output power at a variety of wind speeds up to 15 m/s at fixed resistance. We also measured the rotation rate using a laser tachometer mounted on a metal stand and a piece of reflective tape placed on a blade of the turbine. This testing allowed us to evaluate the turbine's performance and ensure the successful functioning of the system throughout, and our ability to follow the commissioning checklist.

5: References

[1] 2025, “SOLIDWORKS,” Dassault Systèmes [Online]. Available: https://www.3ds.com/products/solidworks.

[2] Pinkerton, R. M., 1937, “Calculated and measured pressure distributions over the MIDSPAN section of the NACA 4412 airfoil - NASA technical reports server (NTRS),” NASA [Online]. Available: https://ntrs.nasa.gov/citations/19930091638.

[3] Polygenis, T., 2023, “How strong is 3D printed plastic: A comprehensive guide,” Wevolver [Online]. Available: https://www.wevolver.com/article/pla-strength.

[4] Chaban, M., 2025, “Isotropic vs. anisotropic strength in 3D printing,” RapidMade [Online]. Available: https://rapidmade.com/isotropic-vs-anisotropic-strength-in-3d-printing/.

[5] Remigius, W., and Natarajan, A., 2021, A review of wind turbine drivetrain loads and load effects for fixed and floating wind turbines [Online]. Available: https://wires.onlinelibrary.wiley.com/doi/epdf/10.1002/wene.417.

[6] Aerodynamics of wind - turbines [Online]. Available: https://geosci.uchicago.edu/~moyer/GEOS24705/Readings/turbine_aerodynamics.pdf.

[7] “Servo - generic (sub-micro size),” SparkFun Electronics [Online]. Available: https://www.sparkfun.com/servo-generic-sub-micro-size.html.

[8] Electricwisers, 2026, “3 phase bridge rectifier – how 6 diodes work?,” electricwisers [Online]. Available: https://www.electricwisers.com/3-phase-bridge-rectifier-working-formula.

[9] Turbine design report - 2024 collegiate wind competition [Online]. Available: https://www.energy.gov/sites/default/files/2024-08/cwc24-turbine-design-report_cal-maritime.pdf

[10] “Arduino Uno REV3,” Arduino Online Shop [Online]. Available: https://store-usa.arduino.cc/products/arduino-uno-rev3?srsltid=AfmBOoq4WDL6fPR3wbdhei7zK3hxS_aSBV-KE3lABWvQwo85PbLjlQnV..